A Pluto-like radius and a high albedo for the dwarf planet Eris from an occultation

Bruno Sicardy, J. L. Ortiz, M. Assafin, E. Jehin, A. Maury, E. Lellouch, R. Gil Hutton, F. Braga-Ribas, Francois Colas, Daniel Hestroffer, et al.

HAL Id: hal-00637720

https://hal.sorbonne-universite.fr/hal-00637720v1

Submitted on 2 Nov 2011

A Pluto-like radius and high albedo for the dwarf planet Eris from an occultation

B. Sicardy[1,2,3], **J. L. Ortiz**[4], **M. Assafin**[5], **E. Jehin**[6], **A. Maury**[7], **E. Lellouch**[1], **R. Gil Hutton**[8], **F. Braga-Ribas**[1,9], **F. Colas**[10], **D. Hestroffer**[10], **J. Lecacheux**[1], **F. Roques**[1], **P. Santos Sanz**[1], **T. Widemann**[1], **N. Morales**[4], **R. Duffard**[4], **A. Thirouin**[4], **A. J. Castro-Tirado**[4], **M. Jelínek**[4], **P. Kubánek**[4], **A. Sota**[4], **R. Sánchez-Ramírez**[4], **A. H. Andrei**[5,9], **J. I. B. Camargo**[5,9], **D. N. da Silva Neto**[9,11], **A. Ramos Gomes Jr.**[5], **R. Vieira Martins**[5,9,10], **M. Gillon**[6], **J. Manfroid**[6], **G. P. Tozzi**[12], **C. Harlingten**[13], **S. Saravia**[7], **R. Behrend**[14], **S. Mottola**[15], **E. García Melendo**[16,17], **V. Peris**[18], **J. Fabregat**[18], **J. M. Madiedo**[19], **L. Cuesta**[20], **M. T. Eibe**[20], **A. Ullán**[20], **F. Organero**[21], **S. Pastor**[22], **J. A. de los Reyes**[22], **S. Pedraz**[23], **A. Castro**[24], **I. de la Cueva**[25], **G. Muler**[26], **I. A. Steele**[27], **M. Cebrián**[28], **P. Montañés-Rodríguez**[28], **A. Oscoz**[28], **D. Weaver**[29], **C. Jacques**[30], **W. J. B. Corradi**[31], **F. P. Santos**[31], **W. Reis**[31], **A. Milone**[32], **M. Emilio**[33], **L. Gutiérrez**[34], **R. Vázquez**[34], **H. Hernández-Toledo**[35]

[1] *LESIA-Observatoire de Paris, CNRS, Univ. Pierre et Marie Curie, Univ. Paris-Diderot, 11, rue Marcelin Berthelot, 92195 Meudon cedex, France.*

[2] *Université Pierre et Marie Curie, 4, Place Jussieu, 75252 Paris cedex 5, France.*

[3] *Institut Universitaire de France, 103, Bld Saint Michel, 75005 Paris, France.*

[4] *Instituto de Astrofísica de Andalucía, CSIC , Apt. 3004, 18080 Granada, Spain.*

[5] *Observatório do Valongo/UFRJ, Ladeira Pedro Antonio 43, CEP 20.080-090 Rio de Janeiro, RJ, Brazil.*

[6] *Institut d'Astrophysique de l'Université de Liège, Allée du 6 Août 17, B-4000 Liège, Belgium.*

[7] *San Pedro de Atacama Celestial Explorations, Casilla 21, San Pedro de Atacama, Chile.*

[8] *Complejo Astronómico El Leoncito (CASLEO) and San Juan National University, Av. España 1512 sur, J5402DSP, San Juan, Argentina.*

[9] *Observatório Nacional/MCT, Rua General José Cristino 77, CEP 20921-400 Rio de Janeiro, RJ, Brazil.*

[10] *Observatoire de Paris, IMCCE, UPMC, CNRS, 77 Av. Denfert-Rochereau, 75014 Paris, France.*

[11] *Centro Universitário Estadual da Zona Oeste, Av. Manual Caldeira de Alvarenga 1203, CEP: 23.070-200 Rio de Janeiro, RJ, Brazil.*

[12] *INAF, Osservatorio Astrofisico di Arcetri, Largo E. Fermi 5, I-50125 Firenze, Italy.*

[13] *Caisey Harlingten Observatory, The Grange, Scarrow Beck Road, Erpingham, Norfolk, NR11 7QX, United Kingdom.*

[14] *Observatoire de Genève, CH-1290 Sauverny, Switzerland.*

[15] *DLR - German Aerospace Center, Rutherfordstr. 2, 12489 Berlin, Germany.*

[16] *Fundació Privada Observatori Esteve Duran, 08553 Seva, Spain.*

[17] *Institut de Ciències de l'Espai (CSIC-IEEC), Facultat de Ciències, Torre C5, 08193 Bellaterra, Spain.*

[18] *Observatori Astronòmic, Universitat de València, C. Catedràtic José Beltrán 2, 46980 Paterna, Spain.*

[19] *Universidad de Huelva, Facultad de Ciencias Experimentales, Av. de las Fuerzas Armadas S/N, 21071 Huelva, Spain.*

[20] *Centro de Astrobiología (CSIC-INTA), carretera de Ajalvir, km 4, 28850 Torrejón de Ardoz, Madrid, Spain.*

[21] *Observatorio astronómico de La Hita, La Puebla de Almoradiel (Toledo), Spain.*

[22] *Observatorio de la Murta, Murcia, Spain.*

[23] *Calar Alto Observatory, Centro Astronómico Hispano Alemán, C/ Jesús Durbán Remón, 2, 04004 Almería, Spain.*

[24] *Sociedad Astronómica Malagueña, Centro Cultural José María Gutiérrez Romero, calle República*

Argentina 9, 29016 Málaga, Spain.

[25] Astroimagen, Abad y Sierra 58, Ibiza, Spain.

[26] Observatorio Nazaret, Nazaret, Lanzarote, Spain.

[27] Liverpool JMU, Twelve Quays House, Egerton Wharf, Birkenhead, CH41 1LD, United Kingdom.

[28] Instituto de Astrofísica de Canarias, Vía Láctea s/n, La Laguna, Tenerife, Spain.

[29] Observatório Astronomico Christus, Colégio Christus, rua João Carvalho 630, Aldeota, CEP 60140-140, Fortaleza, CE, Brazil.

[30] Observatório CEAMIG-REA, CEP31545-120, Belo Horizonte, MG, Brazil.

[31] Departamento de Física - Instituto de Ciências Exatas - Universidade Federal de Minas Gerais, Av. Antônio Carlos 6627, 31270-901 Belo Horizonte, MG, Brazil.

[32] Instituto Nacional de Pesquisas Espaciais (INPE-MCT), Divisão de Astrofísica, Av. dos Astronautas, 1758, São José dos Campos, 12227-010, SP, Brazil.

[33] Universidade Estadual de Ponta Grossa, O.A. - DEGEO, Av. Carlos Cavalcanti 4748, Ponta Grossa 84030-900, PR, Brazil.

[34] Instituto de Astronomía, Universidad Nacional Autónoma de México, Carretera Tijuana-Ensenada, km 103, 22860 Ensenada, B.C., Mexico.

[35] Instituto de Astronomía, Universidad Nacional Autónoma de México, Apartado Postal 70-264, 04510 México D.F., Mexico.

The dwarf planet Eris is a Trans-Neptunian Object (TNO) with an elongated orbit (eccentricity 0.44), a large inclination (44 degrees) relative to the ecliptic plane, and a surface composition very similar to Pluto[1]. It presently resides at 95.7 astronomical units (1 AU is the Earth-Sun distance) from Earth, near its aphelion and more than three times farther than Pluto. Owing to this great distance, measuring its size or detecting a putative atmosphere is difficult. Here we report the observation of a multi-chord stellar occultation by Eris on November 6, 2010 UT. The event is consistent with a spherical shape for Eris, with radius R_E=1,163±6 km, density ρ=2.52±0.05 g cm^{-3} and a high visible geometric albedo p_V=0.96$^{+0.09}_{-0.04}$. No nitrogen, argon or methane atmospheres are detected with surface pressure larger than ~1 nbar, about 10,000 times more tenuous than Pluto's present atmosphere[2]−[5]. As Pluto's radius is estimated[3]−[8] between 1,150 and 1,200 km, Eris appears as a Pluto-twin, with a bright surface possibly caused by a collapsed atmosphere, owing to its cold environment. We anticipate that this atmosphere may periodically sublimate as Eris approaches its perihelion, at 37.8 AU from the Sun.

The dwarf planet (136199) Eris was discovered[9] in 2005. Its radius has been estimated to 1,200±100 km based on direct imaging[10], while its thermal flux detection provided another estimation[11] of 1,500±200 km, potentially making it larger even than Pluto, and the largest known dwarf planet. The motion of Dysnomia (Eris' satellite) provides Eris' mass, M_E=(1.66±0.02)×10^{22} kg, 27% larger than Pluto's mass[12]. No short-term (day scale) brightness variability has been detected for Eris at the 1% level[13],[14], suggesting either a spherical body with no albedo variegation, or − if elongated − a finely-tuned pole-on viewing geometry. Eris spectra is very similar to Pluto and reveals a methane-ice rich cover, and another, dominant ice, presumably nitrogen, but not excluding argon[1].

Stellar occultations by Eris are rare as it subtends a minuscule angular diameter (~0.03 arcsec), while currently moving in severely depleted stellar fields at an angular rate of ~1.5 arcsec hour^{-1} at most. Using the techniques described in ref. [15], we predicted one Eris occultation in 2010, on November 6 UT. We attempted observations from 26 stations, and the occultation was detected from two sites in Chile, with two detections at San Pedro de Atacama (San Pedro for short) with the Harlingten and ASH2 telescopes, 20 metres from each other, and one detection at La Silla, with the TRAPPIST telescope, see Fig. 1 and Supplementary Tables 1S and 2S for details. Another station further south at Complejo Astronómico El Leoncito (CASLEO), Argentina, provided a light curve without occultation, but went close to Eris' shadow edge (~200 km), see Fig. 2.

The San Pedro and La Silla observations provide two occultation segments – or 'chords' –, whose four extremities are used to constrain Eris' size (red segments in Fig. 2). When deriving the occultation times, it appeared that two equally satisfactory solutions for the star re-appearance time at the Harlingten telescope in San Pedro are possible, yielding two different chord lengths. These two solutions are separated by 1.2 s, and are respectively called *solution 1* and *solution 2*, in chronological order. This ambiguity is due to the fact that the star re-appearance occurred during a gap between consecutive exposures, corresponding to a net loss of information. The ASH2 data collected next to Harlingten did not provide enough signal-to-noise ratio to discriminate between these two solutions, and are not used in the fit described below, see Supplementary Information. As a dwarf planet, Eris is expected to be in hydrostatic equilibrium under gravity and centrifugal forces. The most general apparent limb shape is then an ellipse with semiaxes $a'>b'$ with effective radius $R_E=\sqrt{a'b'}$, defined as the radius of a disk that has the same apparent surface area as the actual body. This shape stems either from an oblate Maclaurin spheroid (small angular momentum regime) with an assumed equator-on viewing, or an elongated triaxial Jacobi ellipsoid (large angular momentum regime) observed pole-on, as implied by the absence of brightness variations. We have five free parameters to adjust: a', the apparent flattening $\epsilon'=(a'-b')/a'$, the ellipse position angle P in the sky plane, and the two coordinates of its centre f_c, g_c (Supplementary Table 3S). With four chord

extremities, our observations allow for an infinity of limb solutions. However, as the two chords have almost the same median lines (Fig. 2), this strongly suggests that Eris' shape is indeed close to spherical, unless very special geometries occurred, see below. Using a circular model with three free parameters ($R_E = a'$, f_c, g_c) and adopting solution 2, we obtain $R_E = 1{,}163 \pm 6$ km (1σ formal error). The minimum χ^2 per degree of freedom is $\chi^2_{pdf} = 1.38$ indicates a satisfactory fit to the data, see Supplementary Table 3S. Moreover, the r.m.s. radial residual of 2.1 km is fully consistent with our formal timing errors. We may not exclude, however, that random topographic features with amplitude $\sim \pm 3$ km exist along the limb, which would result in a slightly larger error bar for Eris' radius, $R_E = 1{,}163 \pm 9$ km, see Supplementary Information. Solution 1 provides $R_E = 1{,}140$ km, but with a high value $\chi^2_{pdf} = 30.7$ (5.5σ level), and radial residuals of $+11$ km and -16 km at the beginning and end of the San Pedro chord, respectively. Topographic features of this size are unlikely on such a large icy body. This indicates that the spherical assumption is not correct for solution 1, and explains why we do not provide a formal error bar for that value.

Allowing for a non-zero flattening of Eris' limb, we find an infinity of possible solutions by fixing the position angle P and semi-major axis a' at various values. If Eris' rotation axis and Dysnomia's orbital pole are aligned, we find values of R_E in the range 1,105-1,155 km, smaller than the value 1,163 km derived above. Relaxing the constraint on Eris' orientation, we find that elliptical limb models can satisfactorily fit the occultation chords in 68.3% of the cases (1σ level) for R_E in the range $1{,}165 \pm 90$ km (Supplementary Fig. 4S). However, as R_E departs from 1,165 km, the flattening must rapidly increase, requiring fast rotations which are not supported by observations[13],[14]. The extreme case of $R_E = 1{,}500$ km previously found[11] can be ruled out, as it requires fine tunings in both Eris' limb and pole orientations, see Fig. 2. Thus, the most straightforward interpretation of our observations is that Eris is close to spherical, remembering that larger sizes are possible in a narrow region of the parameter space. Consequently, Eris is close in size to Pluto, whose radius[3]−[8] is estimated between 1,150 and 1,200 km.

Our radius value implies a density of $\rho = 2.52 \pm 0.05$ g cm^{-3}, when combined to Eris' mass[12]. This is comparable to Haumea's density[16],[17] (~ 2.6 g cm^{-3}), for which a typical rock/ice ratio of 0.85/0.15 is derived[18]. This suggests that Haumea (and thus also Eris) is a large rocky body with a thin overlying ice shell. Note that TNOs densities span a large range, with $\rho \sim 1.0$, 1.6 and 2.0 g cm^{-3} for Varuna[17], Charon[19] and Pluto[19], respectively, pointing to diverse origins and/or evolutions. Our radius value provides a geometric albedo of $p_V = 0.96^{+0.09}_{-0.04}$ in the visible, see Supplementary Information. This makes Eris almost as bright as a perfect isotropic Lambert surface (for which $p_V = 1$ by definition), and one of the intrinsically brightest objects of the solar system. For comparison, Saturn's satellite Enceladus is even brighter, with a geometric albedo of $p_V \sim 1.4$, associated with its geologically active surface[20]. In contrast, Eris' brightness and lack of light curve variations may stem from the collapse of a nitrogen atmosphere, see below. We find that Eris is brighter than the TNO 2002 TX$_{300}$, whose high albedo ($0.88^{+0.15}_{-0.06}$) is probably due to the exposition of fresh water-ice[21].

We reassess Eris' surface temperature in the light of our new results. *Spitzer*[22] and *IRAM*[11] measurements imply disk-averaged brightness temperatures of $T_b = 30 \pm 1.2$ K and $T_b = 38 \pm 7.5$ K at 70 and 1,200 μm, respectively. As a completely absorbing surface at Eris' distance has a temperature $T_0 = 40$ K, the second value is surprisingly high (and consistent with the fact that the previously found radius[11] of 1,500 km is about 30% higher than our value), but we note that a unique brightness temperature $T_b \sim 31$ K matches both the *Spitzer* 70 μm and *IRAM* 1,200 μm measurements at the 1.5σ level (Supplementary Fig. 5S). However, Eris' surface temperature is probably not uniform because an atmosphere (if any) would be too tenuous to isothermalise the surface frosts, as occurs for Triton and Pluto. We therefore consider two extreme standard temperature distribution models, corresponding to (1) a warmer slow rotator (or equivalently, pole-on orientation, or zero thermal

inertia, the so-called Standard Thermal Model, STM) with sub-solar temperature T_{ss}, and (2) a cooler fast rotator with equator-on geometry (Isothermal with Latitude Model, ILM), with equatorial temperature T_{eq}.

In the STM, both *Spitzer* and *IRAM* fluxes are reproduced satisfactorily with $T_{ss}{\sim}35$ K (Supplementary Fig. 5S). The thermal equilibrium equation $T_{ss}{=}T_0 \cdot [(1 - p_V q)/(\varepsilon\eta)]^{1/4}$ then provides a relationship between the beaming factor η (describing the effects of surface roughness), the phase integral q and the surface emissivity ε, where $A{=}p_V q$ is the Bond albedo, which measures the fraction of reflected solar energy. Using a standard value[22] $\varepsilon{=}0.9$ and a plausible range from $\eta{=}1$ (no roughness) to 0.7 (large surface roughness), we obtain $q{=}0.49$-0.66, fully consistent with Saturn's brightest icy satellites values[20],[23]. The ILM in contrast leads to the extreme condition $0{<}q{<}0.24$, an implausible range as bright objects also have large phase integrals[24]. Essentially, the fast rotator model does not provide enough thermal flux given the new, smaller size of Eris. We therefore strongly favor the STM, implying either a pole-on orientation or a very small thermal inertia, as observed in other TNOs[25],[26].

The occultation puts an upper limit for a putative Eris' atmosphere. As discussed in the Supplementary Information, our preferred model is an isothermal N_2 atmosphere near 30 K, for which we can place an upper limit of about 1 nbar (1σ level) at the surface, see Fig. 3. Similar limits are obtained for hypothetical CH_4 or Ar atmospheres. Also discussed is the possibiliy that a Pluto-like atmosphere sublimates as Eris approaches its perihelion, at 37.8 AU from the Sun. In that case, Eris would currently be a dormant Pluto twin with a bright icy surface created by a collapsed atmosphere. Detailed models are required, however, to confirm this scenario.

[1] Tegler, S. C. *et al.* Methane and Nitrogen Abundances on Pluto and Eris. *Astrophys. J.* **725**, 1296–1305 (2010).

[2] Yelle, R. V. & Elliot, J. L. in *Pluto and Charon* (eds Stern, S. A. & Tholen, D. J.) 347–390 (Univ. Arizona Press, Tucson, 1997).

[3] Elliot, J.L. *et al.* Changes in Pluto's atmosphere: 1988-2006. *Astron. J.* **134**, 1-13 (2007).

[4] Lellouch, E. *et al.* Pluto's lower atmosphere structure and methane abundance from high-resolution spectroscopy and stellar occultations. *Astron. Astrophys.*, **495**, L17–L21, (2009).

[5] Zalucha, M.A. *et al.* An analysis of Pluto occultation light curves using an atmospheric radiative–conductive model. *Icarus* **211**, 804-818 (2011).

[6] Tholen, D.J. & Buie, M.W. Further analysis of Pluto-Charon mutual event observations. *Bull. Amer. Astron. Soc.* **22**, 1129 (1990).

[7] Young, E.F. & Binzel, R.P. A new determination of radii and limb parameters for Pluto and Charon from mutual event lightcurves. *Icarus* **108**, 186–224 (1994).

[8] Tholen, D.J. & Buie, M.W. in *Pluto and Charon* (eds Stern, S.A. & Tholen, D.J.) 193–219 (Univ. Arizona Press, Tucson 1997).

[9] Brown, M.E., Trujillo, C.A. & Rabinowitz, D.L. Discovery of a Planetary-sized object in the scattered Kuiper Belt. *Astrophys. J.* **635**, L97–L100 (2005).

[10] Brown, M.E., Schaller, E.L., Roe, H.G., Rabinowitz, D.L. & Trujillo, C.A. Direct Measurement of the Size of 2003 UB313 from the Hubble Space Telescope. *Astrophys. J.* **643**, L61–L63 (2006).

[11] F. Bertoldi, F., Altenhoff, W., Weiss, A., Menten, K.M. & Thum, C. The trans-neptunian object UB313 is larger than Pluto. *Nature* **439**, 563–564 (2006).

[12] Brown, M.E & Schaller, E.L. The Mass of Dwarf Planet Eris. *Science* **316**, 1585 (2007).

[13] Sheppard, S. S. *et al.* Light Curves of Dwarf Plutonian Planets and other Large Kuiper Belt Objects: Their Rotations, Phase Functions, and Absolute Magnitudes. *Astron. J.* **134**, 787–798 (2007).

[14] Duffard, R. *et al.* A study of photometric variations on the dwarf planet (136199) Eris. *Astron. Astrophys.*, **479**, 877–881, (2008).

[15] Assafin, M. *et al.* Precise predictions of stellar occultations by Pluto, Charon, Nix and Hydra for 2008-2015. *Astron. Astrophys.* **515**, A32–A45 (2010).

[16] Rabinowitz, M. E. *et al.* Photometric Observations Constraining the Size, Shape, and Albedo of 2003 EL61, a Rapidly Rotating, Pluto-sized Object in the Kuiper Belt. *Astrophys. J.* **639**, 1238-1251 (2006).

[17] Lacerda, P. & Jewitt, D.C. Densities of Solar System Objects from Their Rotational Light Curves. *Astron. J.* **133**, 1393-1408 (2007).

[18] McKinnon, W.B., Prialnik, D., Stern, S.A. & Coradini, A. in *The Solar System beyond Neptune* (eds Barucci, M.A., Boehnhardt, H., Cruikshank, D.P. & Morbidelli, A.) 213–241 (Univ. Arizona Press, Tucson 2008).

[19] Tholen, D. J., Buie, M.W., Grundy, W.M. & T. Elliott, G.T. Masses of Nix and Hydra. *Astron. J.* **135**, 777-784 (2008).

[20] Verbiscer, A., French, R., Showalter, M. & Helfenstein, P. Enceladus: Cosmic Graffiti Artist Caught in the Act. *Science* **315**, 815 (2007).

[21] Elliot, J. L. *et al.* Size and albedo of Kuiper belt object 55636 from a stellar occultation. *Nature* **465**, 897–900 (2010).

[22] Stansberry, J. *et al.* in *The Solar System beyond Neptune* (eds Barucci, M.A., Boehnhardt, H., Cruikshank, D.P. & Morbidelli, A.) 161–179 (Univ. Arizona Press, Tucson 2008).

[23] Howett, C. J. A., Spencer, J. R., Pearl, J. & Segura, M. Thermal inertia and bolometric Bond albedo values for Mimas, Enceladus, Tethys, Dione, Rhea and Iapetus as derived from Cassini/CIRS measurements. *Icarus* **206**, 573–593 (2010).

[24] Brucker, M. J. *et al.* High albedos of low inclination Classical Kuiper belt objects. *Icarus* **201**, 284–294 (2009).

[25] Müller, T. G. *et al.* "TNOs are Cool": A survey of the trans-Neptunian region. I. Results from the Herschel science demonstration phase (SDP). *Astron. Astrophys.* **518**, L146 (2010).

[26] Lellouch, E. *et al.* "TNOs are Cool": A survey of the trans-Neptunian region. II. The thermal lightcurve of (136108) Haumea. *Astron. Astrophys.* **518**, L147 (2010).

Author contributions. B.S. helped plan the campaign, centralised the stellar occultation predictions, participated to the observations, analysed data, wrote and ran the diffraction, limb-fitting and ray-tracing codes, and wrote part of the paper. J.L.O. helped plan the campaign, analysed data for the prediction, participated to the observations, obtained and analysed data, and wrote part of the paper. E.L. analysed the implications of the results for Eris thermal model, albedo constraints and putative atmospheric structure, and wrote part of the paper. M.A., F.B.R., A.H.A., J.I.B.C., R.V.M., D.N.d.S.N. and R.B. discovered the star candidate and analysed data for the predictions. E.J. and A.M. obtained and analysed the positive occultation detection at La Silla/TRAPPIST and San Pedro/Harlingten telescopes, respectively. F.B.R., F.C., M.G. and J.M. analysed data, D.H. calculated Dysnomia position at the moment of occultation and wrote part of the paper. All the other authors participated to the planning of the campaign and/or to the observations, and the authors listed in Supplementary Table 2S were responsible for the observations. All authors were given the opportunity to review the results and comment on the manuscript.

Author information. Correspondence and requests for materials should be addressed to B.S. (bruno.sicardy@obspm.fr).
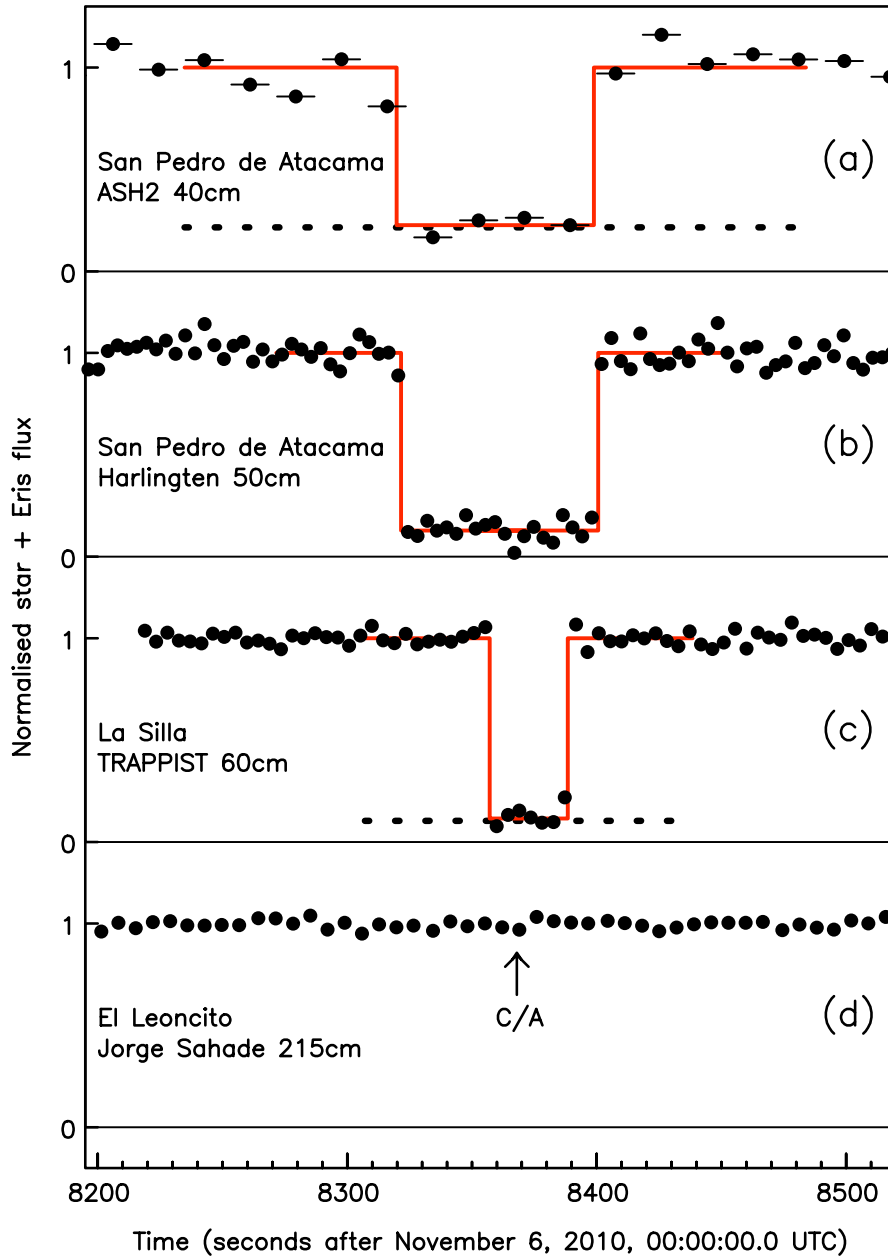
Figure 1 | Eris occultation light curves. The plots show the flux of the star plus Eris, normalised to unity outside the occultation, versus time. No filter was used at any of the telescopes. **a,** The light curve from the ASH2 40-cm telescope at San Pedro de Atacama, using a SBIG STL-11000M CCD camera, with a 2×2 pixel binning and a sub-frame of 11.24×9.71 arcmin (272×235 pixels). The horizontal bars indicate the total time intervals associated with each point (15 s, while the cycle time was 18.32 s). Those bars are too small to be visible on the other data sets. **b,** The light curve from the Harlingten 50-cm telescope at San Pedro de Atacama using an Apogee U42 CCD camera (2×2 pixel binning, sub-frame: 2.67×2.67 arcmin, or 100×100 pixels, integration/cycle times: 3 and 3.88 s). **c,** The light curve from the 60-cm TRAPPIST telescope at La Silla, using a FLI ProLine PL3041-BB CCD camera (2×2 pixel binning, sub-frame: 3.25×3.25 arcmin, or 150×150 pixels, integration/cycle times: 3 and 4.55 s). **d,** The light curve from the 215-cm Jorge Sahade telescope at El Leoncito, using a Roper Scientific Versarray 1300B CCD camera (3×3 pixel binning, sub-frame: 2.62×3.50 arcmin, or 77×103 pixels, integration/cycle times: 4 and 7 s). The horizontal dotted lines at the bottom of the ASH2 and TRAPPIST light curves represent Eris' contribution to the flux, showing that the star completely disappeared during the event, see Supplementary Section 2. The red lines are the best square-well models fitted to the events. We show here the solution 2 for the Harlingten light curve (the solution 1 being very close at that scale, see Supplementary Fig. 3S). The vertical arrow in panel (d) shows the time of closest approach (C/A) to the shadow edge at CASLEO, at 8368 s UT.
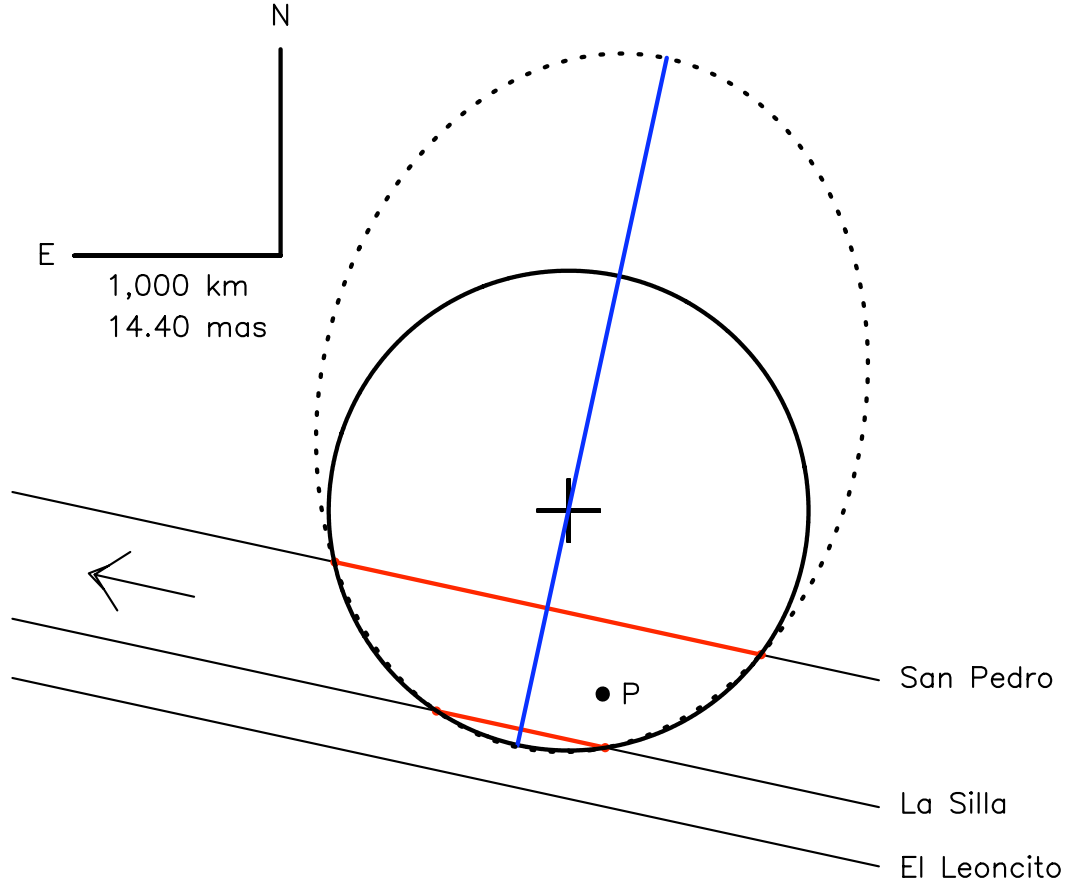
Figure 2 | Measuring Eris' size. The three oblique solid lines show the star trajectories relative to Eris, as seen from San Pedro de Atacama, La Silla and CASLEO, with the arrow pointing toward the direction of motion. The San Pedro and La Silla timings provide the lengths of the two occultation segments, or 'chords' (in red), see solution 2 in Supplementary Table 3S. The median lines of the two red segments are separated by only 5 km and coincide at that scale with the blue line. Celestial north is up and east is left. The scale in kilometres and milli-arcsec (mas) is shown, with one mas corresponding to 69.436 km at Eris. The solid circle has a radius R_E=1,163 km and is our preferred solution for Eris' size and shape, with the cross marking the position of the centre. The dot near 'P' indicates Dysnomia's orbit pole direction[12] projected onto Eris' surface. The dotted curve is an elliptic limb fitted to our occultation chords, with semi-major and -minor axes of a'=1708 and b'=1317 km, respectively, i.e. an apparent effective radius of R_E=1500 km, the value of Eris' radius previously derived from thermal measurements[11]. The long axis of the ellipse should be perpendicular to the occultation chords to within ±2 degrees in order to match our data points. This has a low probability of 2% to occur for a random limb orientation between 0 and 180 degrees. Furthermore, the ellipse has an aspect ratio b/a=0.771 that would require a fast rotator (with a period of 4.4 hours) observed pole-on to within 18 degrees to suppress rotational light curve[13],[14]. This has also a low probability of 5% to occur for a randomly distributed pole orientation, making the dotted limb solution unlikely.
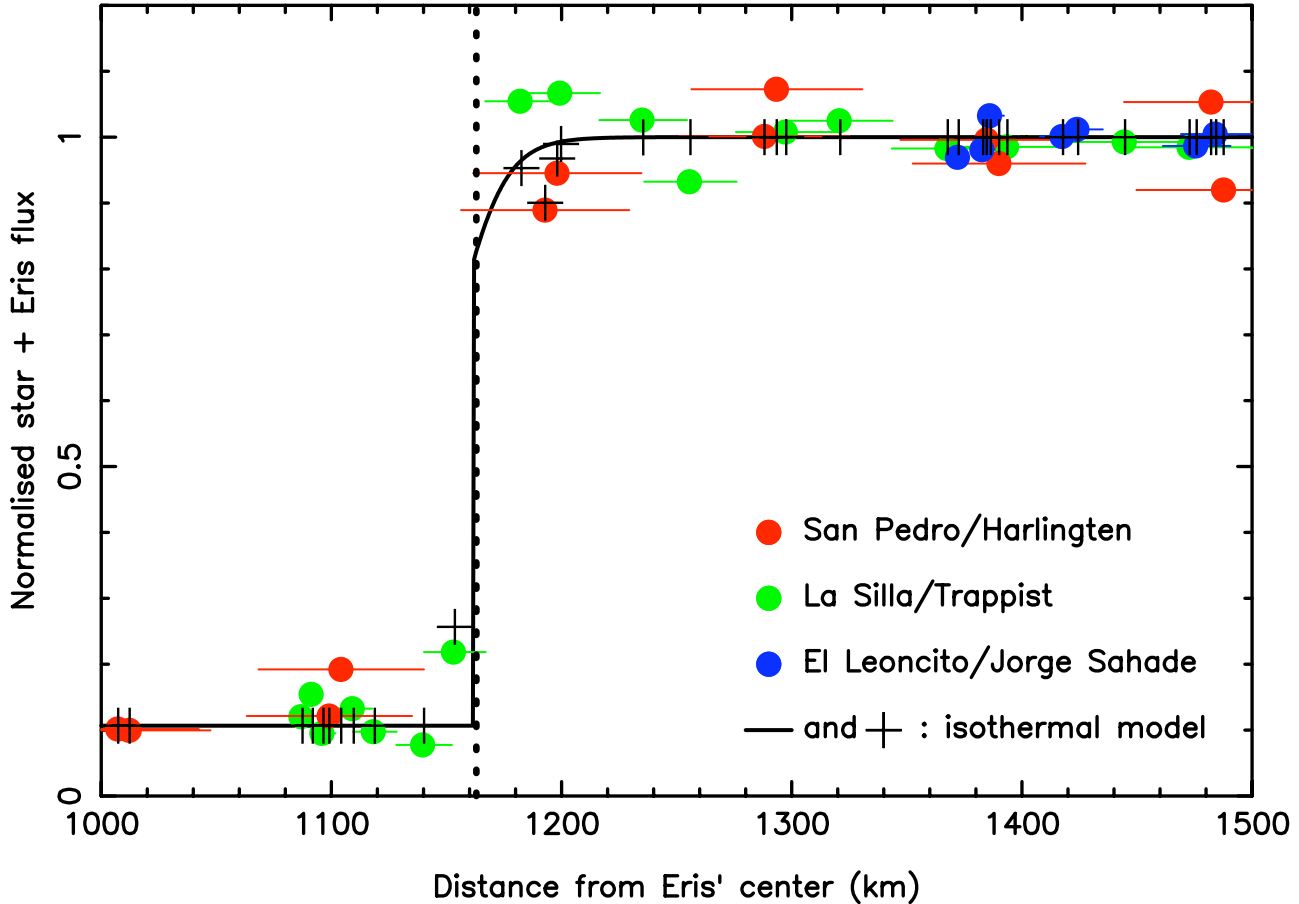
Figure 3 | Upper limit on Eris' atmosphere. Each data point (colored bullets) obtained at three of the stations shown in Fig. 2 has been projected onto a radial scale (distance from Eris' centre), using the circular solution 2 displayed in Fig. 2. The horizontal bars indicate the finite radial resolution associated with finite integration intervals, while the vertical dotted line shows the adopted Eris radius, R_E=1,163 km. The black solid line is a model light curve obtained at 1-km resolution, using an isothermal pure N_2 atmosphere. Black crosses mark the expected flux associated with each data point, once the convolution with the finite integration intervals has been performed. The fit minimises the differences between the black crosses and the corresponding data points (bullets). The model shown here is the 3σ-level upper limit of an isothermal N_2 atmospheric profile, with T=27.7 K and surface pressure of 2.9 nbar. Most of the constraint on the model comes from the two data points obtained at La Silla (the two green bullets just right of the vertical dotted line) corresponding to the data points obtained just before and just after the event (Fig. 1). The two closest San Pedro data points in red have only a small contribution to the χ^2 value, while the CASLEO data points in blue are too far away from Eris' edge ($\sim$200 km) to effectively constrain the atmospheric pressure. Using solution 1 instead of solution 2 for Eris shape would have a minimal impact on the atmospheric upper limit, as this would slightly displace the San Pedro data points in the plot, leaving the La Silla points where they are shown here.